ELSEVIER

Chemical Geology 216 (2005) 89–97

CHEMICAL GEOLOGY
INCLUDING
ISOTOPE GEOSCIENCE

www.elsevier.com/locate/chemgeo

Effect of Mn(II) incorporation on the transformation of ferrihydrite to goethite

Mariana Alvarez[a], Elsa E. Sileo[b], Elsa H. Rueda[a,*]

[a]*Departamento de Química, Universidad Nacional del Sur, Av. Alem 1253, B8000CPB, Bahía Blanca, Argentina*
[b]*INQUIMAE, Departamento de Química Inorgánica, Analítica y Química Física, Facultad de Ciencias Exactas y Naturales, Universidad de Buenos Aires, Pabellón II, Ciudad Universitaria, C1428EHA, Buenos Aires, Argentina*

Received 14 January 2004; accepted 2 November 2004

Abstract

A series of Mn-substituted goethites were obtained by the addition of Mn(II) to ferrihydrite in alkaline media, at different times. The total aging period was 24 h. Chemical analysis indicated that the Mn mol fraction (χ_{Mn}) remained practically constant (ca. 8 mol%) in the oxalate–ammonium non-extracted samples. In the extracted samples, the χ_{Mn} values increased with the earlier addition of the Mn(II) solution to the iron–oxyhydroxide suspension.

XRD patterns of the obtained solids showed that the unique phase present was goethite. Although, in most of the experiments, the Mn(II) was added when the goethite phase was already formed, variations in the unit cell parameters were observed. The changes in the cell parameters followed the trend reported for coprecipitated samples. An enlargement of the acicular crystals is in line with the higher Mn incorporation. Lattice parameters and cell volume for the extracted samples were obtained by the Rietveld simulation of XRD data.

Kinetics measurements indicate that the initial dissolution rate increases with the Mn content in the goethite structure, except in the samples where Mn was added later. Dissolution–time curves show a better fit with the two-dimensional contracting geometry law than with the cubic root law, this fact is attributed to the presence of two more exposed faces, both of different reactivity, in the acicular crystals of the Mn-substituted goethite. The dissolution has also well been described by the Kabai equation. Deviation from congruence indicates an inhomogeneous distribution of Mn into the goethite crystals due to the more belated addition of Mn to the solid phase.

Keywords: Goethite; Mn-substituted goethites; Acid kinetics; Lattice parameters

1. Introduction

Iron oxides are common products that form over the earth's surface under several environmental conditions. Naturally occurring goethite is unlikely to

* Corresponding author. Tel.: +54 291 4595159.
E-mail address: ehrueda@criba.edu.ar (E.H. Rueda).

0009-2541/$ - see front matter © 2004 Elsevier B.V. All rights reserved.
doi:10.1016/j.chemgeo.2004.11.004

exist as pure α-FeOOH and usually has incorporations of different foreign elements (Gerth, 1990). Soil goethite may contain substantial amounts of Al (up to 33 mol%) by isomorphous substitution of Fe^{3+} ion in the octahedral sites (Davey et al., 1975; Fitzpatrick and Schwertmann, 1982; Lewis and Schwertmann, 1979; Schulze, 1984). Other cations, such as chromium (Schwertmann et al., 1989), manganese (Stiers and Schwertmann, 1985) cobalt and nickel (Lim-Nuñez and Gilkes, 1987; Carvalho-e-Silva et al., 2003) and germanium (Bernstein and Waychunas, 1987) can also be incorporated into the structural framework of the oxyhydroxide. Since conversion of ferrihydrite to goethite in alkaline media occurs by dissolution and reprecipitation processes, its formation is strongly influenced by the presence of foreign ions and molecules. In general, foreign species tend to stabilize ferrihydrite against dissolution. However, Mn promotes dissolution of ferrihydrite facilitating the nucleation/growth of goethite (Cornell and Giovanoli, 1987). In some systems, the crystal morphology is also modified.

Manganese is an important element in the aquatic environment and is a subject of much interest because its oxides scavenge other heavy metals. This element can exist in a number of oxidation states, the II, III, and IV states being important in natural waters. Mn and Fe are mobilized and precipitated in soils and sediments over a similar range of redox potentials (Patrick and Jugsujinda, 1992). But reports on Mn-substituted goethite from soils or marine crusts are scarce. In the laboratory, α-$Mn_xFe_{1-x}OOH$ can be easily synthesized in alkaline media from Mn(III) or Mn(II) salts, with manganese mol fraction (χ_{Mn}=Mn/(Mn+Fe)) up to 0.13 (Stiers and Schwertmann, 1985; Vandenberghe et al., 1986; Cornell and Giovanoli, 1987; Diaz et al., 1989; Vempati et al., 1995; Ford et al., 1997; Gasser et al., 1999; Sileo et al., 2001). High substitution of Fe-by-Mn, χ_{Mn} near to 0.47, can be achieved when crystallization is carried out at acid pH (Ebinger and Schulze, 1989; Ebinger and Schulze, 1990). Ferrimagnetic (Fe, Mn) spinel phases form at a pH≥8 (Ebinger and Schulze, 1990; Wolski et al., 1997; Sileo et al., 2001). Karim (1984) showed that the presence of Mn lowers the crystallinity of goethite formed from slow oxidation of $FeCl_2$ solutions at pH 7.

X-ray absorption and diffraction techniques were used to study the structural environment and oxidation state of Mn in goethite–groutite solid solutions, α-$Mn_xFe_{1-x}OOH$, with $\chi_{Mn}\leq 0.47$ (Scheinhost et al., 2001). X-ray absorption near-edge structure (XANES) studies carried out in these samples revealed that only Mn(III) is present in goethite regardless of whether the samples were derived from Mn(II) or Mn(III) solutions. This behaviour has two implications: first, Mn(II) was oxidized by one step to Mn(III) at the surface of the growing crystals, and second, the incorporation of this Mn(III) into the growing goethite crystals proceeds faster than the disproportion of Mn(III) to Mn(II) and Mn(IV). Then, Mn(III) incorporated in the solid phase may be more stable than trivalent Mn in solution, and consequently more frequent in the environment than expected.

Rietveld refinement (Rietveld, 1969) of X-ray diffraction data was employed to investigate the statistical long-range structure. The results suggest that increasing χ_{Mn} leads to gradual elongation of the average Fe, Mn octahedron that causes an increase of the lattice *a* parameter and a decrease of *b* and *c* parameters in line with Vegard's law. (Scheinhost et al., 2001; Sileo et al., 2001).

Iron oxides present low solubility in pure water (Schwertmann, 1991), however, their dissolution process could be promoted by acid attack and by action of chemical or bacterial reductive reagents (Bousserrhine et al., 1999). The presence of complexant agents in the reaction media is also important. Lim-Nuñez and Gilkes (1987) showed that Mn-substituted goethites and goethites substituted with other transition metals dissolve at rates different from that of pure goethite.

Dissolution kinetics have been used to describe the mechanism of release of cations incorporated in natural iron oxides (Singh and Gilkes, 1991). Besides, they can offer an indication about the effects of the Mn incorporation on the solubility and stability of minerals in soils environment.

This paper presents the analysis of the influence of Mn(II) incorporation at different ferrihydrite aging times, through the structural study of the final solid phase and kinetics results of acid dissolution of different samples. A comparison between these oxides and those obtained from

Table 1
Chemical composition of Mn-substituted goethites with and without ammonium oxalate-treatment

Unextracted samples				Extracted samples			
Sample	Fe[a]	Mn[a]	χ_{Mn}=Mn/(Mn+Fe)	Sample	Fe[a]	Mn[a]	χ_{Mn}=Mn/(Mn+Fe)
E_0	1.0469	0.0958	0.0838	E'_0	0.9309	0.0871	0.0856
E_4	1.1025	0.0995	0.0828	E'_4	1.0863	0.0531	0.0466
E_8	1.0725	0.0935	0.0802	E'_8	1.0644	0.0413	0.0374
E_{12}	1.0439	0.0968	0.0849	E'_{12}	1.0348	0.0332	0.0311
E_{16}	1.0525	0.0952	0.0829	E'_{16}	1.0394	0.0287	0.0269
E_{20}	1.1453	0.0980	0.0804	E'_{20}	1.1445	0.0192	0.0165

[a] Expressed as mol/100 g sample.

ferrihydrite coprecipitated with both metals is also performed.

2. Materials and methods

Samples of goethite were synthesized as described by Stiers and Schwertmann (1985). Six samples were prepared by adding aqueous $Fe(NO_3)_3.9H_2O$ (45 cm^3, 0.53 mol dm^{-3}) to NaOH (175 cm^3, 2.00 mol dm^{-3}). The precipitate was centrifuged, washed twice with bidistilled water and aged at 333 K for 24 h in a NaOH solution (250 cm^3, 0.30 mol dm^{-3}). $Mn(NO_3)_2.4H_2O$ (5 cm^3, 0.53 mol dm^{-3}) was added to this solution, at different times: 4, 8, 12, 16 and 20 h (samples E_4, E_8, E_{12}, E_{16} and E_{20}, respectively). A blank of pure goethite (sample B) and a new sample E_0, obtained by the simultaneous precipitation of manganese and iron cations, were prepared similarly. The final solids were washed, dried and gently crushed. In order to remove poorly crystalline compounds from precipitates, half of each solid was extracted in the dark with ammonium oxalate (0.2 mol dm^{-3}, pH 3.0) for 4 h. The other half was used non-extracted. The non-extracted and the extracted samples were identified as E_i and E'_i (with $0<i<20$), respectively.

The Mn and Fe contents of the solids were determined by atomic absorption spectrometry (AAS) with a GBC Model B-932 spectrometer. Absorption analysis was made by duplicate on 20 mg of each sample dissolved in 100 cm^3 HCl (6 mol dm^{-3}, 333–353 K).

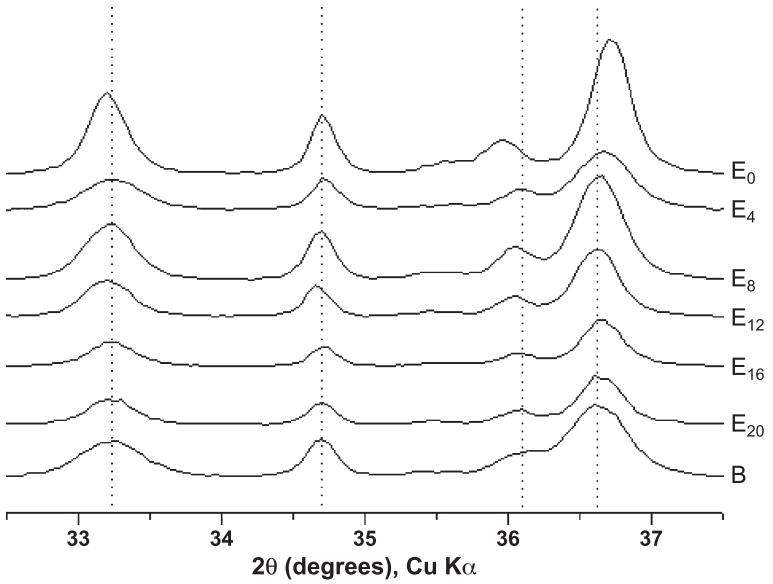

Fig. 1. XRD patterns for goethite samples with different Mn contents (2θ range: 31.5–37.5°), showing shift in XRD.

Particle morphologies were obtained by scanning electron microscopy (SEM) using a Philips SEM 515 equipment operated at 30 keV. Samples for SEM were dispersed in bidistilled water with ultrasonic treatment and a drop of suspension was placed onto a metallic support.

X-ray diffraction (XRD) patterns were recorded in a Siemens D5000 diffractometer using a CuKα radiation. Generator settings were 40 kV, 30 mA. Divergence, scattered and receiving slits were 1°, 1° and 0.2 mm, respectively. A curved graphite monochromator was used. Data were collected in the 2θ range: 18.5–135.0°, with scanning step of 0.025° and a counting time of 20 s per point. The step width assured a minimum of about 12 intensity points for the narrower peaks. The data were analyzed using the GSAS (Larson and Von Dreele, 1994) system. Starting unit-cell parameters and atomic coordinates for goethite were taken from the literature (Szytula et al., 1968). Peak profiles were fitted using the Thompson–Cox–Hastings pseudo-Voigt function (Thompson et al., 1987).

Dissolution kinetics were performed in air in a sealed cylindrical beaker provided with a thermostat water jacket and measured at 303 K. 100 mg of each sample was suspended in HCl (50 cm^3, 6 mol dm^{-3}) and the suspension was magnetically stirred throughout the experiment. The dissolution reaction was followed by measuring the amount of Fe and Mn released at regular time intervals. 1 cm^3 aliquots were withdrawn, from the suspension and filtered with a syringe through a Nuclepore membrane (pore size 0.22 μm). Previous dissolution studies used a solution to solid ratio in the range 250–2000:1 (Cornell et al., 1974; Sidhu et al., 1981; Lim-Nuñez and Gilkes, 1987) to ensure that dissolution was independent of the solution to sample ratio (Cornell et al., 1974; Sidhu et al., 1981). In this work, the solution to solid ratio was 500:1. Determinations of dissolved Fe and Mn amounts were performed by AAS. All the kinetic experiments were carried out in duplicate.

3. Results and discussion

3.1. Chemical and physical analysis of the solids

Table 1 shows the results of chemical analysis of the samples before and after the ammonium oxalate extraction. The χ_{Mn} in the non-extracted series remains essentially constant indicating a leveling off in the total uptake (adsorption and substitution) of Mn ions.

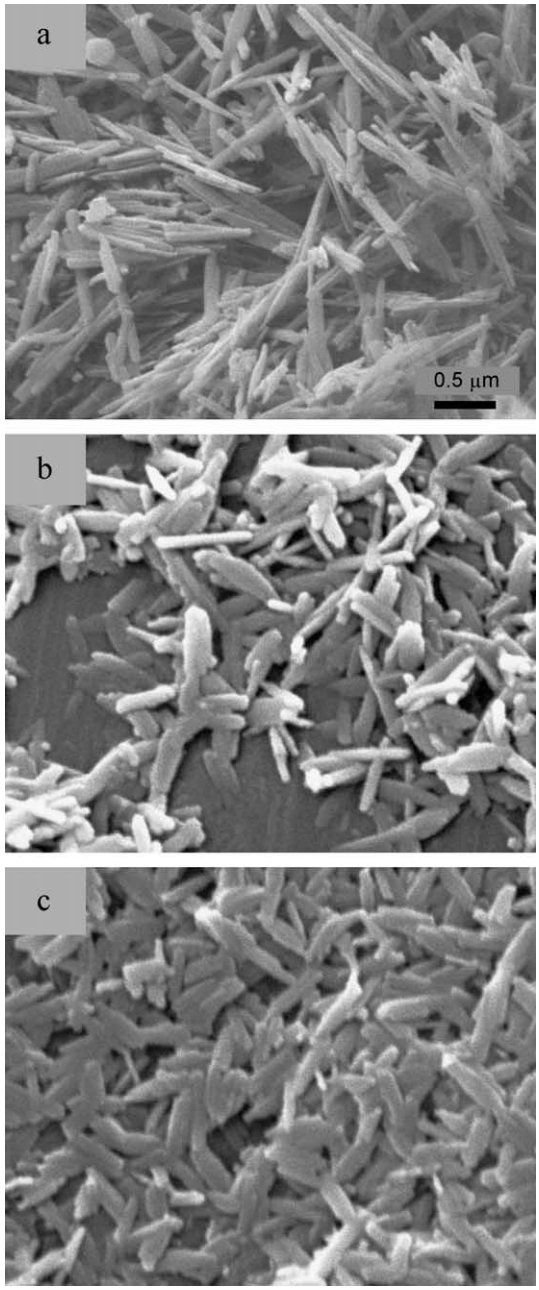

Fig. 2. Scanning electron micrographs for samples (a) E_0, (b) E_{12} and (c) E'_{12}.

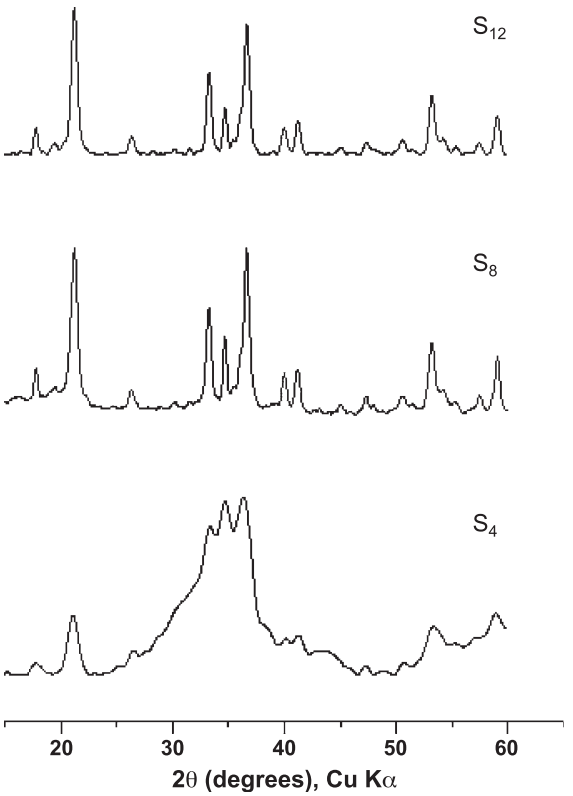

Fig. 3. XRD patterns of Fe(III) precipitated species just before the Mn(II) addition.

In the untreated samples, the Mn mol fraction remained practically constant (ca. 8%). However in the extracted samples, the χ_{Mn} value decreases from E_0 to E_{20}, indicating that the amount of Mn incorporated into the structure increases with the earlier addition of the $Mn(NO_3)_2$ solution to the iron solid phase.

Fig. 1 presents the XRD patterns of the unextracted samples.

The diagrams correspond to an unique goethite-like phase. The peak displacements displayed indicate variations in the unit cell parameters due to Mn incorporation into the goethite structure. Since, XRD patterns do not show the presence of any other crystalline phase, the Mn non-incorporated into the structure of goethite would form an amorphous oxide over the goethite surface. The amorphous phase is not detected by SEM images; the micrographs for the extracted and non-extracted samples are almost identical. Fig. 2 displays the morphologies of E_0, E_{12} and E'_{12}. An enlargement of the acicular crystals in E_0 is ascribed to the higher Mn incorporation.

Fig. 3 shows the XRD profiles of the different oxyhydroxides just before the Mn incorporation with aging times of 4, 8 and 12 h (identified as S_4, S_8 and S_{12} samples). Only in sample S_4, Mn is added to ferrihydrite. From samples S_8 to S_{20}, Mn addition is carried out when the goethite phase has already formed.

3.2. Structural change and lattice parameters of substituted samples

Lattice parameters and cell volume obtained in the Rietveld refinement of the various samples are shown in Table 2. Fig. 4 shows the variations of the cell parameters vs. Mn substitution for these samples, and a comparison with a series of coprecipitated Mn-goethites (G_i, with $0<i<0.073$) obtained in an earlier work (Sileo et al., 2001).

According to preliminary data (Stiers and Schwertmann, 1985; Sileo et al., 2001), the *a*- and *c*-

Table 2
Unit cell dimensions of Mn-substituted goethites obtained by the Rietveld method

Sample	χ_{Mn}	GoF/R_{wp} R_{exp}/R_{Bragg}	*a* (nm)	*b* (nm)	*c* (nm)	Volume (nm^3)
E_0	8.53	1.15; 7.65; 5.74;3.42	0.45996(1)	0.99853(2)	0.30187(1)	0.138645(04)
E_4	4.65	1.24; 9.93; 7.53; 13.41	0.46142(5)	0.99611(5)	0.30216(1)	0.138878(10)
E_8	3.74	1.21; 8.12; 6.24; 3.59	0.46143(2)	0.99590(3)	0.30224(1)	0.138892(09)
E_{12}	3.11	1.18; 9.46; 7.18; 4.29	0.46144(2)	0.99586(3)	0.30226(1)	0.138895(15)
E_{16}	2.69	1.17; 12.33; 9.58; 5.71	0.46145(4)	0.99578(5)	0.30227(1)	0.138894(18)
E_{20}	1.65	1.11; 11.59; 8.66; 4.50	0.46150(2)	0.99562(4)	0.30244(1)	0.138966(07)
B	0.00	1.15; 7.35; 5.53; 3.97	0.46183(3)	0.99553(4)	0.30256(1)	0.139062(07)

Values in parentheses are esd for the least significant figures of the data shown, the esd values are taken from the final cycle of the Rietveld refinement.

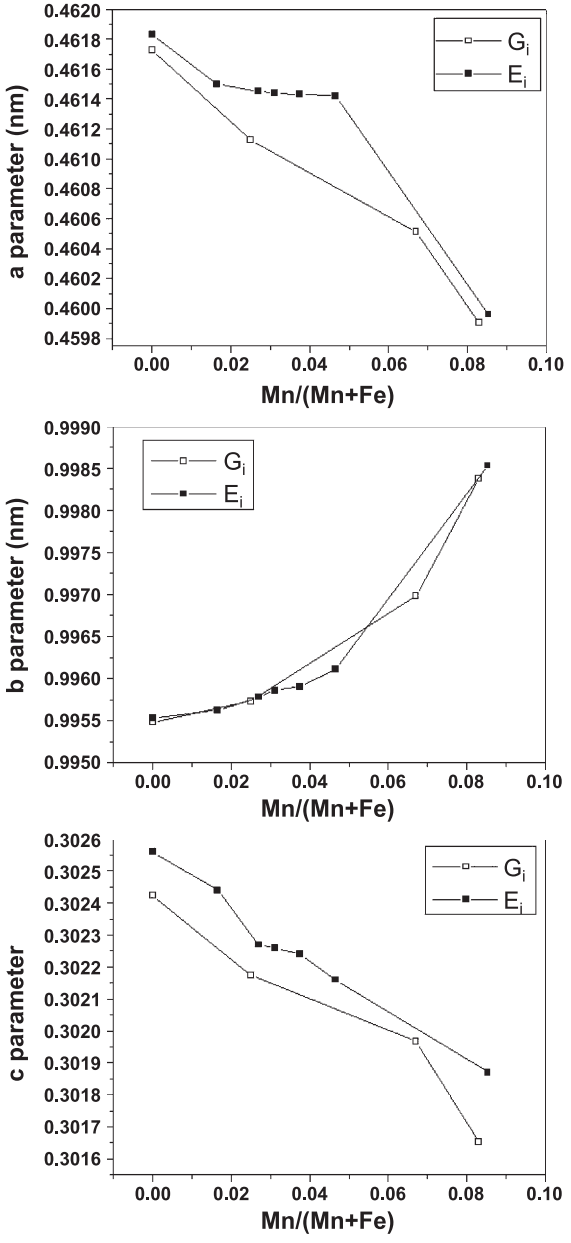

Fig. 4. Lattice parameters vs. Mn content in the Mn-substituted goethites previously extracted with ammonium oxalate.

parameters decrease and the *b*-parameter increases with the increment of χ_{Mn}. From E'_4 to E'_{20}, the changes are small and the greatest changes are detected in E'_0. Cell parameters for samples E'_4 to E'_{20} are slightly different from those of sample B (pure goethite). The comparison between E'_0 and the other samples denote the influence of coprecipitation vs. the belated addition of Mn(II) to the oxyhydroxide, in the uptake of Mn in the crystal framework. Substitution is markedly higher in E'_0 where the Mn(II) and Fe(III) are coprecipitated . The comparison of data for the G series (aging time 21 days) and the E′ series (aging time 24 h) indicates that only the *a*-parameter shows meaningful variations with the aging time.

3.3. Kinetics of acid dissolution

The kinetic profiles of total Fe released vs. time for samples treated with ammonium oxalate are shown in Fig. 5. Dissolution curves from E_8 to E_{20} show sigmoidal shapes, while the curves for the samples with greater Mn content show deceleratory shapes, which are similar to dissolution curves of goethite obtained by Cornell et al. (1975) and Lim-Nuñez and Gilkes (1987). The same trend is observed for oxides without oxalate-extraction (not shown).

Initial dissolution rates (R_0), measured as $(\mathrm{dFe\ (mol\ g^{-1})}/\mathrm{d}t)_{t=0}$ were used to explore the influence of χ_{Mn} on the rates of dissolution. In general, as shown in Table 3, the samples with the highest values of χ_{Mn} show the highest values of R_0 in both types of samples. This fact indicates that Mn(III) substantially unstabilizes goethite against proton attack. Similar behaviour was also reported by Lim-Nuñez and Gilkes (1987), and Schwertmann (1991) and could be attributed to the octahedral

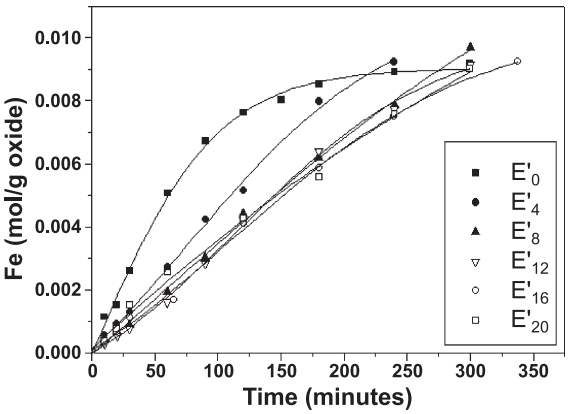

Fig. 5. Iron concentration vs. time curves for the oxalate-extracted samples dissolved in 6 mol dm^{-3} HCl at 303 K.

Table 3
Comparison of initial dissolution rates of Mn-substituted goethites with and without oxalate treatment

Sample	Initial rate (R_0) (mol g^{-1})	N	R^2	Sample	Initial rate (R'_0) (mol g^{-1})	N	R^2
E_0	1.81×10^{-4}	7	0.987	E'_0	1.10×10^{-4}	11	0.997
E_4	7.11×10^{-5}	9	0.999	E'_4	3.83×10^{-5}	9	0.998
E_8	5.34×10^{-5}	10	0.997	E'_8	3.47×10^{-5}	10	0.999
E_{12}	5.12×10^{-5}	9	0.999	E'_{12}	2.60×10^{-5}	10	0.998
E_{16}	4.82×10^{-5}	8	0.995	E'_{16}	2.77×10^{-5}	9	0.998
E_{20}	6.45×10^{-5}	8	0.997	E'_{20}	4.79×10^{-5}	9	0.998

E'_i indicates oxides oxalate-extracted.

distortion produced by Mn(III) substitution, generating an enlargement of the two axial Mn–(O,OH) distances. The comparison of the same sample with and without ammonium oxalate treatment indicates that the initial dissolution rate is generally greater in the untreated sample. This result is attributed to the presence of an amorphous phase covering the crystalline particles of Mn-goethites.

The increment of the initial rate observed in samples E'_{16} and E'_{20} suggests that the Mn is mainly incorporated in the outer layers of the particles forming a layer of Mn-rich goethite (more soluble) that facilitates the acid dissolution.

Iron and manganese analysis of sequential extracts during the dissolution of samples can provide information regarding the distribution of Mn(III) within the structure of goethite. Preliminary work by Sidhu et al. (1981) showed that convex or concave %Me vs. %Fe curves indicate accumulation of the incorporated metal at the surface or towards the core of goethite crystals, respectively. By contrast, a straight line of unit slope intersecting the origin suggests that metal ions are uniformly incorporated within goethite. Fig. 6 compares the evolution of the manganese and iron dissolved fractions, $f_M=w/w_0$ (where w is the mass of dissolved metal at time t and w_0 is the initial mass). The convex curves for samples E_4 to E_{20} (Fig. 6) indicate that Mn tends to be concentrated towards the surface of particles. For instance, in samples E_{16} and E_{20} when $f_{Mn}=0.8$, $f_{Fe}<0.05$. Only in E_0 the release of Mn and Fe is roughly congruent indicating that both ions are uniformly distributed in the particles. The shapes of the curves show that the distribution of Mn into the particles is more uniform when the elapsed

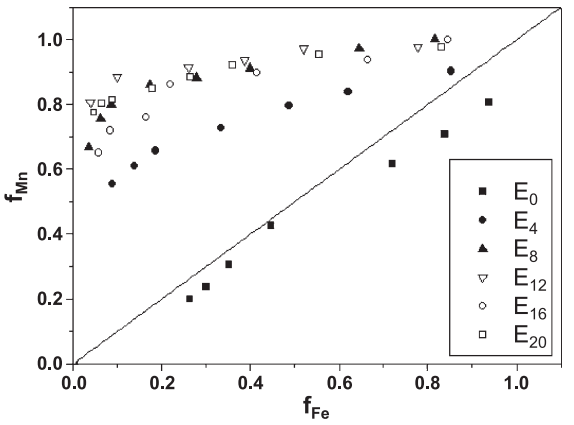

Fig. 6. Plots of fraction of dissolved Mn vs. fraction of dissolved Fe for the oxalate unextracted samples. Solid line of unit slope indicates uniform incorporation of metal ions within goethite.

time between ferrihydrite precipitation and Mn addition is shorter.

Samples with the ammonium oxalate treatment (Fig. 7) show a greater congruency in the dissolution behaviour, except for E'_{20}, where the later Mn incorporation generates a minor and inhomogeneous incorporation.

The acicular crystals of goethite present two more exposed faces: (110) and (021) planes, both of different reactivity (Barrón and Torrent, 1996). Rueda et al. (1992) have shown that the two-dimensional contracting geometry kinetic law is more adequate to describe the acid dissolution of the goethite than the

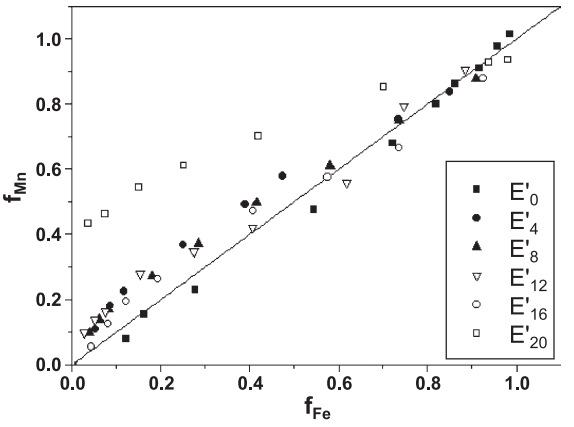

Fig. 7. Plots of fraction of dissolved Mn vs. fraction of dissolved Fe for the oxalate-extracted samples. Solid line of unit slope indicates uniform incorporation of metal ions within goethite.

cubic law. The two-dimensional contracting model follows the law:

$$1 - \sqrt{(1-f)} = kt \quad (1)$$

where k is the rate constant (time^{-1}). The rate constants for the different extracted samples (E'_i) are summarized in Table 4.

As a general rule, the rate constant values diminish as the Mn content in the solid decreases. The value for E'_{20} higher than E'_{12} is also in line with the presence of a Mn-rich goethite layer on the surface of the particles in the latter sample.

Sigmoidal dissolution–time profiles may also be well described by the equation of Kabai (1973):

$$f = 1 - e^{-(kt)^{\alpha}} \quad (2)$$

k and α are constants that can be obtained from a linear transformation of Eq. (2):

$$\ln\ln[1/(1-f)] = \ln k' + \alpha \ln t \quad (3)$$

where $k'=\alpha \ln k$. The equation of Kabai is an extension of the pseudomonomolecular-reaction equation where α becomes unity; correlation coefficients >0.99 were obtained for all experimental data, except for sample E_0 (R^2=0.95). In this case, two straight lines provided the best fit (R^2=0.99). The k values obtained by Kabai equation show the same decreasing trend that those calculated form Eq. (1). Wells et al. (2001) found for Mn-substituted hematites that their experimental data could be fully described by Kabai equation when Mn content was 6.3 mol% but did not extended to hematite containing 3.3 mol% Mn, this may be due to an inhomogeneous distribution of the host in the oxide structure. Although the Kabai equation provides a flexible way of summarizing experimental data, it is not based on any fundamental conceptual model of the dissolution process and therefore does not provide any physical meaning (Cornell and Schwertmann, 1996).

Table 4
Dissolution rate constant for dissolution–time profiles fitted to the quadratic rate equation

Sample	k	N	R^2
E'_0	0.00354	11	0.926
E'_4	0.00253	9	0.995
E'_8	0.00212	10	0.988
E'_{12}	0.00209	10	0.993
E'_{16}	0.00206	9	0.995
E'_{20}	0.00280	9	0.995

4. Conclusions

The Mn incorporation into the goethite structure is higher when Mn is added to ferrihydrite samples. However, addition of Mn after precipitation of the solid phase led to a partial and inhomogeneous incorporation of original Mn(II), depending of the interaction time. It is important to emphasize that Mn can be adsorbed and then incorporated in the previously formed goethite.

Changes in unit cell dimensions of goethite are consistent with the amount of manganese incorporated in unextracted samples. These changes are less significant than those observed in samples synthesized by Fe–Mn coprecipitation (Fig. 7).

Comparison between E'_i and G_i samples (obtained by coprecipitation in an earlier work) showed the same trend in the variation of the cell parameters, but this variation is smaller for the E'_i series.

The two-dimensional contracting geometry law and the rate equation of Kabai successfully described the acid dissolution of E'_i samples.

Acknowledgements

This work has been partially supported by SGCyT-PGI: 24/Q005, Universidad Nacional del Sur, Bahía Blanca, and GRANT-UBACYTX-168, 2004–2007, from Universidad Nacional de Buenos Aires. **[LW]**

References

Barrón, V., Torrent, J., 1996. Surface hydroxyl configuration of various crystal faces of hematite and goethite. J. Colloid Interface Sci. 177, 407–410.

Bernstein, L.R., Waychunas, G.A., 1987. Germanium crystal chemistry in hematite and goethite from Apex Mine, Utah, and some data on germanium in aqueous solution and in stollite. Geochim. Cosmochim. Acta 51, 623–630.

Bousserrhine, N., Gasser, U.G., Jeanroy, E., Berthelin, J., 1999. Bacterial and chemical reductive dissolution of Mn-, Co-, Cr-, and Al-substituted goethites. Geomicrobiol. J. 16, 245–258.

Carvalho-e-Silva, M.L., Ramos, A.Y., Tolentino, H.C., Enzweiler, J., Netto, S.M., Martin Alves, M.C., 2003. Incorporation of Ni into natural goethite: an investigation by X-ray absorption spectroscopy. Am. Mineral. 88, 876–882.

Cornell, R.M., Giovanoli, R., 1987. Effect of manganese on the transformation of ferrihydrite into goethite and jacobsite in alkaline media. Clays Clay Miner. 35, 11–20.

Cornell, R.M., Schwertmann, U., 1996. The iron oxides. Structure, properties, reactions, occurrence and uses. VCH, Weinheim (Federal Republic of Germany). 573 pp.

Cornell, R.M., Posner, A.M., Quirk, J.P., 1974. Crystal morphology and the dissolution of goethite. J. Inorg. Nucl. Chem. 36, 1937–1946.

Cornell, R.M., Posner, A.M., Quirk, J.P., 1975. The complete dissolution of goethite. J. Appl. Chem. Biotechnol. 25, 701–706.

Davey, B.G., Rusell, J.D., Wilson, M.J., 1975. Iron oxide and clay minerals and their relation to colours of red and yellow podzolic soils near Sydney, Australia. Geoderma 14, 125–138.

Diaz, C., Furet, N.R., Nikolaev, V.L., Rusakov, V.S., Cordeiro, M.C., 1989. Mössbauer effect study of Co, Ni, Mn and Al bearing goethites. Hyperfine Interact. 46, 689–693.

Ebinger, M.H., Schulze, D.G., 1989. Mn-substituted goethite and Fe-substituted groutite synthesized at acid pH. Clays Clay Miner. 37, 151–156.

Ebinger, M.H., Schulze, D.G., 1990. The influence of pH on the synthesis of mixed Fe–Mn oxide minerals. Clay Miner. 25, 507–518.

Fitzpatrick, R.W., Schwertmann, U., 1982. Al-substituted goethite—an indicator of pedogenic and other weathering environment in South Africa. Geoderma 27, 335–347.

Ford, R.G., Bertsch, P.M., Farley, K.J., 1997. Changes in transition and heavy metal partitioning during hydrous iron oxide aging. Environ. Sci. Technol. 31, 2028–2033.

Gasser, U.G., Nüesch, R., Singer, M.J., Jeanroy, E., 1999. Distribution of Mn in synthetic goethite. Clay Miner. 34, 291–299.

Gerth, J., 1990. Unit-cell dimensions of pure and trace metal-associated goethites. Geochim. Cosmochim. Acta 54, 363–371.

Kabai, J., 1973. Determination of specific activation energies of metal oxides and metal oxide hydrates by measurement of the rate dissolution. Acta Chim. Acad. Sci. Hung. 78, 57–73.

Karim, Z., 1984. Influence of transition metals on the formation of iron oxides during the oxidation of $Fe(II)Cl_2$ solution. Clays Clay Miner. 32, 334–336.

Larson, A.C., Von Dreele, R.B., 1994. GSAS. General structural analysis system. Los Alamos Natl. Lab. Rep. LAUR 86, 748.

Lewis, D.G., Schwertmann, U., 1979. The influence of Al on the formation of iron oxides: preparation of Al-goethites in M KOH. Clay Miner. 14, 115–126.

Lim-Nuñez, R., Gilkes, R.J., 1987. Acid dissolution of synthetic metal containing goethites and hematites. Proceedings of the International Clay Conference, 1985. The Clay Minerals Society, Bloomington, Indiana, pp. 187–204.

Patrick Jr., W.H., Jugsujinda, A., 1992. Sequential reduction and oxidation of inorganic nitrogen, manganese, and iron in flooded soil. Soil Sci. Soc. Am. J. 56, 1071–1073.

Rietveld, H.M., 1969. A profile refinement method for nuclear and magnetic structures. J. Appl. Crystallogr., B 25, 925–946.

Rueda, E.H., Ballesteros, M.C., Grassi, R.L., Blesa, M.A., 1992. Dithionite as dissolving reagent for goethite in the presence of EDTA and citrate. Application to soil analysis. Clays Clay Miner. 40, 575–585.

Scheinhost, A.C., Stanjek, H., Schulze, D.G., Gasser, U., Sparks, D.L., 2001. Structural environment and oxidation state of Mn in goethite–groutite solid-solutions. Am. Mineral. 86, 139–146.

Schulze, D.G., 1984. The influence of aluminum on iron oxides: unit-cell dimensions of Al-substituted goethites and estimation of Al from them. Clays Clay Miner. 32, 36–44.

Schwertmann, U., 1991. Solubility and dissolution of iron oxides. Plant Soil 130, 1–25.

Schwertmann, U., Gasser, U., Sticher, H., 1989. Chromium-for-iron substitution in synthetic goethites. Geochim. Cosmochim. Acta 53, 1193–1197.

Sidhu, P.S., Gilkes, R.J., Cornell, R.M., Posner, A.M., Quirk, J.P., 1981. Dissolution of iron oxides and oxyhydroxides in hydrochloric and perchloric acids. Clays Clay Miner. 29, 269–276.

Sileo, E.E., Alvarez, M., Rueda, E.H., 2001. Structural studies on the manganese for iron substitution in the goethite–jacobsite system. Int. J. Inorg. Mater. 3, 271–279.

Singh, B., Gilkes, R.J., 1991. Properties and distribution of iron oxides and their association with minor elements in the soils of south-western Australia. J. Soil Sci. 43, 77–98.

Stiers, W., Schwertmann, U., 1985. Evidence for manganese substitution in synthetic goethite. Geochim. Cosmochim. Acta 49, 1909–1911.

Szytula, A., Burewicz, A., Dimitrijevick, Z., Krasnicki, S., Rzany, H., Todorovic, J., et al., 1968. Neutron diffraction studies of α-FeOOH. Phys. Status Solidi 26, 429–434.

Thompson, P., Cox, D.E., Hastings, J.B., 1987. Rietveld refinement of Debye–Scherrer synchrotron X-ray data from Al_2O_3. J. Appl. Crystallogr. 20, 79–83.

Vandenberghe, R.E., Verbeeck, A.E., DeGrave, E., Stiers, W., 1986. ^{57}Fe Mössbauer effect study of Mn-substituted goethite and hematite. Hyperfine Interact. 29, 1157–1160.

Vempati, R.K., Morris, R.V., Lauer, H.V., Helmke, P.A., 1995. Reflectivity and other physicochemical properties of Mn-substituted goethites and hematites. J. Geophys. Res. 100, 3285–3295.

Wells, M.A., Gilkes, R.J., Fitzpatrick, R.W., 2001. Properties and acid dissolution of metal-substituted hematites. Clays Clay Miner. 49, 60–72.

Wolski, W., Wolska, E., Kaczmarek, J., Piszora, P., 1997. Ferrimagnetic spinels in hydrothermal and thermal treatment of $Mn_xFe_{2-2x}(OH)_{6-4x}$. J. Therm. Anal. 48, 247–258.